# Formation of multiple filamentation in a high-power femtosecond laser pulse under rain conditions

**V.P. Kandidov and V.O. Militsin**

*M.V. Lomonosov Moscow State University*

Received April 5, 2006

The influence of the coherent scattering by rain droplets on the multiple filamentation generation in a femtosecond sub-TW laser pulse has been studied numerically. Qualitative agreement between simulation results and data of field experiment is shown. Based on the results of spectral analysis of the beam intensity distribution, the influence of aerosol concentration and radiation power on dimensions of the filament generation areas and their formation mode was investigated.

## Introduction

At present, the high-power femtosecond laser radiation propagation in the atmosphere has aroused a considerable interest. The reason is in a wide range of applications connected with nonlinear effects arising under conditions of a high power light field of a supershort laser pulse. Some of these applications are the laser sensing and monitoring of atmosphere, detection of impurities in gas composition and aerosol, laser-induced emission spectroscopy, control for breakdown in air for atmospheric electricity discharge, and so on.[1]

The interaction of high-power femtosecond laser radiation with the atmosphere as a multicomponent medium comprises a variety of problems. One of them is stochastic multifilamentation in pulses of terawatt power,[2] which can be caused both by the initial beam fluctuations[3] or the refractive index fluctuations in the turbulent atmosphere[4] and by the scattering and absorption of radiation by atmospheric aerosol particles.

The aerosol particles themselves in the intense light field are of interest,[5,6] as well as caused by them variations in the character of pulse propagation through the aerosol medium. The experimental[7] and theoretical[8] works are known devoted to the process of filamentation in a pulse incident on individual particles. The authors show that the filament remains stable if there is a droplet or a solid absorbing disk approximately as large as the filament transverse size (~100 μm) in its path.

The influence of absorption in a dense aerodisperse medium on the filamentation of high-power laser pulses was investigated in laboratory experiments.[9,10] It was shown that nonlinear interaction with aerosol of high density did not affect significantly the radiation energy characteristics. At the same time, the effect of the aerosol with a high extinction coefficient on the pulse filamentation is equivalent to the linear extinction. To describe experimental data, a model is proposed in Ref. 10, in which particles are replaced by absorbing disks, and the scattered radiation component is not taken into account. This model can represent variations in the filamentation mode due to the pulse energy decrease. The effect of highly absorbing aerosol layer on the generated filament length was investigated numerically in Ref. 11.

However, the effect of scattering by the atmospheric aerosol on the femtosecond laser pulse filamentation remains poorly studied. The first qualitative results on the laser pulse filamentation in the fine rain were obtained in 2005 in the field experiment in New Mexico.[12] The diffraction pattern typical for scattering by spherical particles was observed in the pulse cross section.

Of considerable interest is theoretical investigation of the generation process of the laser pulse multifilamentation in the presence of atmospheric aerosol, in particular, fog or rain. Basically, in this case there occurs the light scattering in a forward direction, because the most probable particle size in the rain, as well as in most types of clouds and fogs significantly exceeds the radiation wavelength. Under these conditions the scattered component remains in the beam and may be sufficiently large. When interfering with unperturbed field, there occur small-scale distortions in the pulse cross section. The beam profile perturbations due to the scattering may be centers of development of the radiation modulation instability in the medium with the Kerr nonlinearity,[13] and, hence, regions of the multifilamentation generation. Thus, the aerosol particles become the reason for a significant variation in the femtosecond pulse propagation mode, namely, the occurrence of multifilamentation.

The proposed in Ref. 14 stratified model of radiation propagation in the aerodispersion medium allows one to describe physical processes, which take place when high-power laser radiation crosses aerosol, and to estimate the aerosol particle effect on the filamentation process.

In this paper, the effect of the coherent scattering by rain droplets on the multifilamentation in a subterawatt power pulse is described. A qualitative agreement between the simulation results and the field experiment data[12] is demonstrated. The spectral analysis of the intensity distribution has been performed

0235-6880/06/09 686-07 $02.00 

under different initial conditions, that made it possible to determine the scales of the filamentation areas and the mode of their occurrence.

## The model of the pulse filamentation in the fine rain

The analysis of nonlinear optical interaction of laser radiation with rain droplets is based on the stratified model of the radiation propagation.[14] The model consists of a series of screens with particles coherently scattering the radiation, which results in a small-scale intensity redistribution in a beam. At free areas between aerosol screens the diffraction and nonlinear-optical pulse interaction with gas components of air take place. The interference of a scattered component with unperturbed field causes intensity fluctuations in the pulse cross section. At areas of free propagation between screens these perturbations can become centers of filament generation due to radiation self-focusing in air.

We consider the influence of water droplet coherent scattering on the filament generation, that is, the initial filamentation stage preceding the laser plasma generation. Prior to the attainment of the photoionization threshold, the power redistribution in the temporal pulse layers is caused by the Kerr focusing, which determines the spatial location of filaments. At the initial filamentation stage the nonlinear defocusing in plasma, as well as energy losses for ionization can be neglected, because the electron generation occurs only after attainment of the photoionization threshold in a nonlinear focus. Besides, we can ignore the dispersion of group velocity and the variation of time front steepness of a pulse, because these processes affect the pulse variation in time and are insignificant when analyzing the filament incipience.[4] Hence, variation of the field $E(x, y, z)$ between aerosol screens results from the stationary small-scaled beam self-focusing with perturbations caused by the droplet scattering. In this case, the beam power $P$ coincides with the peak power $P_{\text{peak}}$ of the femtosecond pulse, which value determines the distance to the filamentation start point. In accordance with the accepted approximations, the equation for the complex field amplitude $E(x, y, z)$ at the initial stage of filamentation has the form:

$$2ik\frac{\partial E(x,y,z)}{\partial z} = \frac{\partial^2 E}{\partial x^2} + \frac{\partial^2 E}{\partial y^2} + \frac{2k^2}{n_0} n_2 |E|^2 E(x,y,z) + \\ + \hat{D}_{\text{aer}} E(x,y,z), \qquad (1)$$

where $k$ is the wave number; $n_2$ is the air nonlinearity coefficient; $\hat{D}_{\text{aer}}$ is the operator describing the field transformation due to the coherent scattering by screen particles. Equation (1) does not take into account the effect of a nonlinear response delay due to the stimulated scattering at rotational transitions of nitrogen and oxygen molecules. At the initial stage of filamentation this delay results in the increase of the distance to the filament origin, which can be taken into account by introducing the effective nonlinearity coefficient $n_{2\text{eff}}$.[15]

In the numerical simulation, a $8a \times 8a$ calculation grid was used ($a$ is the initial Gaussian beam radius), containing 4096×4096 nodes in the plane of the pulse cross section. A smoothly increasing absorption was introduced at the grid boundaries in order to eliminate the field components scattered at a large angle to the propagation direction from the region under study. Equation (1) at regions of free propagation was solved in the spectral space with adaptively variable integration step $\Delta z_{\text{nl}}(z)$ of $z$. Aerosol screens were located with a uniform step $\Delta z_{\text{aer}}$. When calculating the Kirchhoff integral to determine the field scattered by a particle of aerosol screen of d$z$ thickness, the local screen grid was used, which step was by 3 orders of magnitude less than the particle diameter. The field obtained as a result of scattering was interpolated to the calculation grid. It was assumed that the field variation on the droplet aperture was insignificant.

For qualitative comparison and assignment to real parameters, we used the data of the field experiment[12] on the study of propagation of a femtosecond terawatt laser pulse (a beam of 2.5 TW, 150 fs, 3 cm) along the atmospheric path under conditions of drizzle at a ~3200 m height above the sea level. Figure 1 shows the energy density distribution in the cross section of an individual pulse recorded in this experiment.

**Fig. 1.** The energy density distribution of an individual pulse in the plane of its cross section.[12] The path length is 75 m, the particle concentration $n \sim 1.7 \cdot 10^4$ m$^{-3}$.

Several dark spots in the distribution correspond to larger energy concentrations in the pulse cross section. The occurrence of randomly located "hot" points is typical for the multifilamentation regime of a laser pulse.[10] At the same time, the concentric rings, which are not connected with the generated filaments, earlier were not observed. In the authors' opinion, these rings represent the result of energy redistribution due to the diffraction at individual

aerosol particles, occurred in the immediate vicinity of the plane of recording.

The estimated particle concentration $n$ in the rain based on the experimentally measured value of the absorption coefficient $\alpha \sim 6.6$ km$^{-1}$, is $\sim 1.7 \cdot 10^4$ m$^{-3}$. If to use the estimation of the extinction coefficient for monodispersion aerosol

$$\alpha = 2\pi R^2 n, \qquad (2)$$

then such a value at the given concentration corresponds to the rain consisting of droplets of the radius $R \sim 250$ μm. Note that the polydispersion distribution of droplets of radii between 0.1 and 0.5 mm takes place in actual drizzles.[16]

In the numerical investigation we considered the radiation of the peak power $P_{\text{peak}} = 100P_{\text{cr}}$ at $\lambda = 800$ nm, where the critical power $P_{\text{cr}}$ of self-focusing in air was $\sim 3$ GW.[17] The initial beam had the Gaussian profile:

$$I(x, y \mid z = 0) = I_0 \exp\left[-(x^2 + y^2)/a^2\right] \qquad (3)$$

at $a = 1.5$ cm; in this case the initial peak intensity $I_0$ corresponding to the given power is $\approx 4.2 \cdot 10^8$ W/cm$^2$.

To study the effect of rain droplets on the pulse filamentation, we considered the monodispersion aerosol at $n \sim 1.7 \cdot 10^4$ m$^{-3}$ and $R = 150$ μm. The attenuation coefficient at the chosen parameters was $\sim 2.4$ km$^{-1}$. Thus, the parameters, used in the numerical simulation, corresponded to data of the *in situ* experiment.[12]

The stratified model was used in the calculations, in which the distance between aerosol screens $\Delta z_{\text{aer}}$ was 1 m, the screen thickness d$z$ was 5 cm. The initial step of integration $\Delta z_{\text{nl}}(0)$ was 10 cm, and later on it was decreased by a factor of two at more than $\pi/5$ increase of the phase incrusion due to the Kerr nonlinearity. Hence, 50 aerosol screens with statistically independent particle distribution were located on a path of 50 m length. At the chosen $n \sim 1.7 \cdot 10^4$ m$^{-3}$ the mean number of droplets $M$ on the screen was about 250, that, recalculated to the circle of the beam radius, gave about 12 droplets.

## Results of numerical experiments

Intensity distributions $I(x, y)$ in the cross section of the pulse central layer, obtained in the numerical experiment under different conditions of propagation, are shown in Fig. 2 as tone images, where a darker tone corresponds to a higher intensity. The path length was about 50 m in all cases.

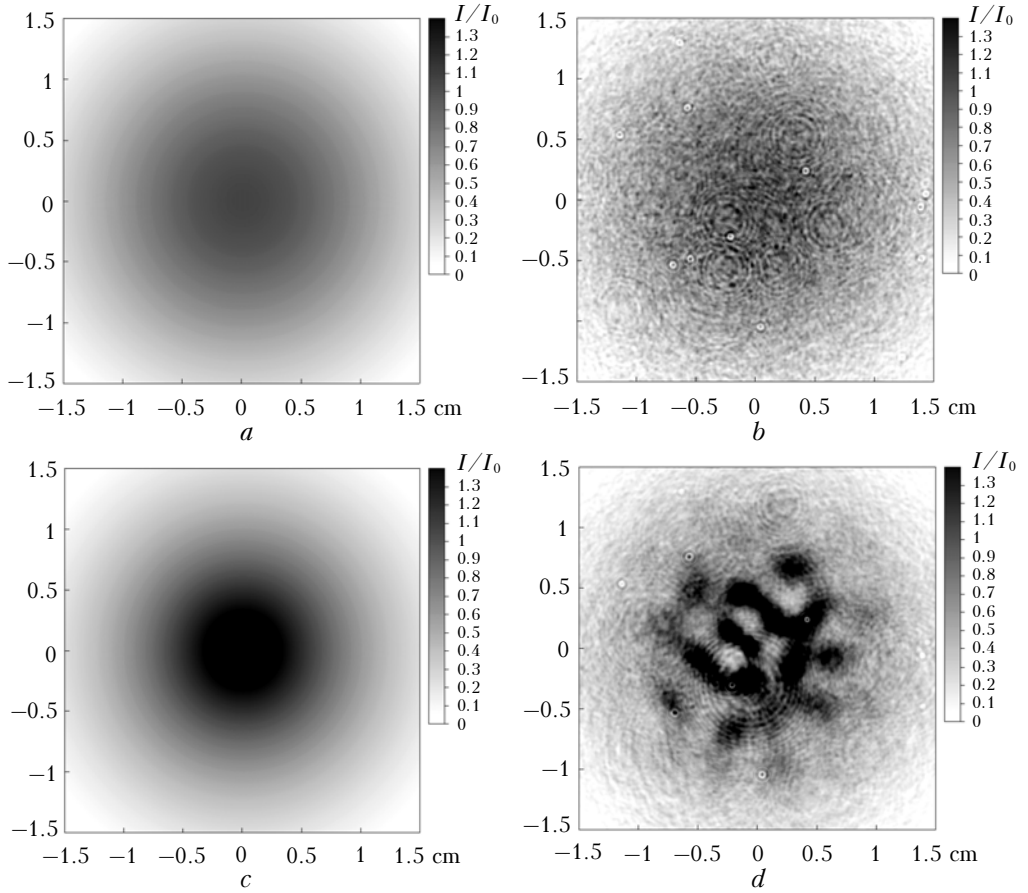


**Fig. 2.** Intensity distribution $I(x, y)$ under the following conditions: only diffraction (*a*); in the presence of aerosol at $n \sim 1.7 \cdot 10^4$ m$^{-3}$ and $R = 150$ μm (*b*); accounting for the Kerr nonlinearity at $P_{\text{peak}} = 100P_{\text{cr}}$ (*c*); simultaneously under conditions (*b*) and (*c*) (*d*).

Figure 2*a* shows the intensity distribution in the cross section of a low-power pulse propagating in the absence of nonlinearity and the rain. This distribution, only due to the diffraction spread along the path equal to 0.03 diffraction beam length, can be used further for comparison as a reference one.

Figure 2*b* shows the characteristic intensity distribution derived in the numerical experiments at propagation of a low-power laser beam in the rain, i.e., in the absence of the air Kerr nonlinearity. The presented distribution, obtained for an individual realization of statistically independent aerosol screens with randomly located particles, corresponds to the short-exposure recording, at which rain droplets can be considered as fixed.

It is seen that the coherent scattering by particles results in small-scaled beam distortions. Against the background of the speckle-pattern, characteristic ring structures are observed resulted from the radiation scattering by individual rain droplets located at the path end. The statistical averaging of the numerical experiment data over an ensemble of 10 realizations has given a $(\sim 7 \pm 1)\%$ relative decrease of intensity in the axial beam region. When using the exponential extinction law and the above-mentioned value of the absorption coefficient (2), the intensity decrease on the beam axis due to aerosol particle scattering is about 11%. The divergence between the experimental and theoretical results is explained by the fact that the scattering by rain droplets is mainly in the forward direction and the scattered radiation remains in the beam. For this reason the use of the Bouguer law with the coefficient derived by Eq. (2), gives an overestimated value of the radiation extinction. This fact is discussed in detail in Ref. 14.

The simulation pattern of the radiation propagation under conditions of the Kerr self-focusing in air without rain is given in Fig. 2*c*. The axially symmetric pattern of the beam self-focusing as a whole is seen, at which the intensity in the near-axial region exceeds the initial one by a factor of 1.5 at a distance of 50 m. This result agrees with the estimate of a beam self-focusing distance $z_{sf}$ as a whole, which follows from the Marburger formula[18]:

$$z_{sf} = \frac{0.367ka^2}{\left\{\left[\left(P/P_{cr}\right)^{1/2} - 0.852\right]^2 - 0.0219\right\}^{1/2}}. \quad (4)$$

By this estimate, when the beam of $P = 100P_{cr}$ propagates along the path in the absence of turbulence and aerosol, the distance of global self-focusing $z_{sf}$ is 70.9 m. Thus, in the presence of the Kerr nonlinearity, the global beam contraction due to self-focusing takes place as compared to the case of only linear diffraction and the beam regular structure conservation — as compared to the aerosol case. In this case, the intensity increase at a distance of 50 m along the axis at the self-focusing is still insignificant.

Consider the origination and the character of multifilamentation in case of femtosecond radiation propagation in rain. It is well-known that the distortions in the high-power pulse cross section in the Kerr medium result in the beam decomposition due to modulation instability.[13] Figure 2*d* shows the typical intensity distribution $I(x, y)$ at laser pulse self-focusing in the air in the presence of rain droplets, obtained in some realizations.

A complex pattern of the intensity distribution is a consequence of small-scale radiation self-focusing under conditions of overlapping of interference patterns from randomly located scattering centers. A considerable energy redistribution in the cross section plane is observed, which is typical for generation of a large number of filaments in a laser pulse. In this case, in the central part, where the intensity in "hot" points increases due to the small-scale beam self-focusing, the regions with low intensity occur as well. The energy from these regions due to the Kerr nonlinearity in the cross section plane has moved to the adjacent maxima, where further the development of filaments is expected. Analysis of the presented distribution has shown that at a distance of 50 m the intensity at six "hot" points is 2–10 times higher than the initial peak value. This significantly exceeds the intensity growth in the absence of aerosol.

Figure 2*d* shows that the disposition of droplets in aerosol screens agrees with their distribution in the case presented in Fig. 2*b*. Note that some diffraction rings under self-focusing conditions are more contrast, because droplets, which caused the scattering, occurred in the region of the increased intensity, and the perturbations, produced by them, increase due to the modulation instability.

If to compare the obtained intensity variation in a pulse in the presence of aerosol and the Kerr nonlinearity (Fig. 2*d*) with the case of its propagation in the absence of rain (Fig. 2*c*), then it may be concluded that distortions, caused by the droplet scattering, are favorable for the occurrence of small-scale self-focusing, which progresses more rapidly than the beam global self-focusing (see Eq. (4)).

The calculated intensity distribution (Fig. 2*d*) qualitatively well agrees with the experimental one[12] (Fig. 1).

## Spatial spectrum of laser radiation at the initial stage of filamentation in rain

Consider the intensity spatial spectrum in the pulse cross section to analyze the influence of small-scale random distortions, caused by the laser radiation scattering by rain droplets, on the filament origination. The spectrum can afford the information about the distortion scales prevailing in the beam, as well as about the portion of radiation power spent for the distortions. The spectrum variation with the distance allows one to study the formation of regions of a possible incipience of filaments.

The spatial intensity spectrum $F_I(z_m; k_x, k_y)$ at a set of distances $z_m$ was calculated using the two-dimensional Fourier transform of intensity distribution $I(z_m; x, y)$ derived from individual realizations of the numerical experiment:

$$F_I(z_m;k_x,k_y) = \hat{F}\{I(z_m;x,y)\}, \qquad (5)$$

where $\hat{F}$ is the operator of two-dimensional Fourier transform.

Since rain droplets are characterized by the homogeneous distribution in the considered region, and the problem is statistically axially-symmetrical, then it is convenient in the analysis to pass from the two-dimensional intensity spectrum $F_I(k_x, k_y)$ to the one-dimensional $F_I(k)$ with the space frequency corresponding to the radial coordinate $r$:

$$F_I(z_m;k) = \frac{1}{\sigma_k}\iint\limits_{\sigma_k} \left|F_I(z_m;k_x,k_y)\right| \mathrm{d}k_x \mathrm{d}k_y. \qquad (6)$$

where $\sigma_k$ is the ring region in the plane of wave vectors, limited by the radii $k$ and $k + \Delta k$. Procedure (6) is equivalent to the additional averaging, possible due to the statistical axial symmetry of results.

To obtain the statistically reliable result, the calculated $F_I(z_m; k)$ was averaged over an ensemble of 10 random realizations of aerosol path in the rain. The statistical analysis was performed at different values of laser beam power and monodispersion aerosol concentration $n$ at $R = 150$ μm. The initial beam profile was Gaussian (3) of radius $a = 1.5$ cm.

To analyze the effect of scattering in the rain on the intensity spectrum, the spatial spectrum of the beam self-focused in air in the absence of aerosol was taken as a reference one. Figure 3 shows $F_I(k)$ at $P = 100P_{cr}$ and $z_m = 1$, 50, 60, and 69.4 m.

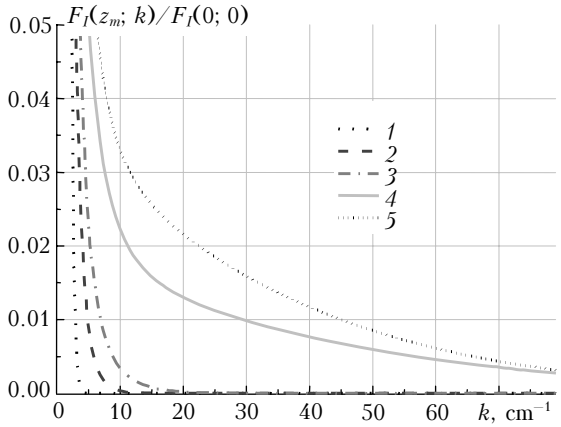


**Fig. 3.** The variation of the beam intensity spatial spectrum $F_I(z_m; k)/F_I(0; 0)$ at self-focusing in the absence of aerosol. Curves correspond to $z_m$ = 1 m (*1*), 50 (*2*), 60 (*3*), and 69.4 m (*4*) at $P = 100P_{cr}$; 102.2 m (*5*) at $P = 50P_{cr}$. The relative error does not exceed 1%.

The selected distances are determined by the beam self-focusing length $z_{sf}$, which, according to Eq. (4), in this case is 70.9 m. The spectra are normalized to the density $F_I(0; 0)$ in the beginning of the path at $k = 0$. At the same time, for convenience of the analysis, the spectrum wing responsible for the change of space scales in the intensity distribution at self-focusing is given in detail. In the numerical experiment the radiation propagation was simulated up to $L_{max} = (69.4 \pm 0.1)$ m, where the peak intensity 100 times exceeded the initial $I_0$.

Figure 3 shows that the initial Gaussian beam ($z_m = 1$ m) has a narrow spatial spectrum, in which only low-frequency ($k < 5$ cm$^{-1}$) components, determined by its initial radius, are significant. Further, as the distance increases, high-frequency components grow and the spectrum widens due to formation of a narrow intensity peak at the self-focusing.

At $L_{max}$ close to the self-focusing distance $z_{sf}$, two spatial scales exist. Low-frequency harmonics ($k < 10$ cm$^{-1}$) characterizing the scale of the beam as a whole increase by several times between 60 and 69.4 m, whereas high-frequency harmonics ($k > 30$ cm$^{-1}$) increase by several orders of magnitude. This points to the fact that at $100P_{cr}$ the size of the beam as a whole decreases insignificantly due to the self-focusing, and an avalanche-like increase of a narrow peak takes place at its axis. As the power decreases to $50P_{cr}$, the spatial spectrum harmonics increase with the distance uniformly along all over the frequency axis (see Fig. 3). At an equal excess of the initial intensity, relative influence of low-frequency harmonics becomes stronger than at $100P_{cr}$, that corresponds to a greater compression of the beam as a whole.

The presence of rain droplets qualitatively changes the spatial spectrum form in a beam. Figure 4 shows the spatial spectrum for a set of $z_m$ at $n = 1.7 \cdot 10^3$ m$^{-3}$ obtained by averaging over the ensemble of 10 realizations at a beam power of $100P_{cr}$.

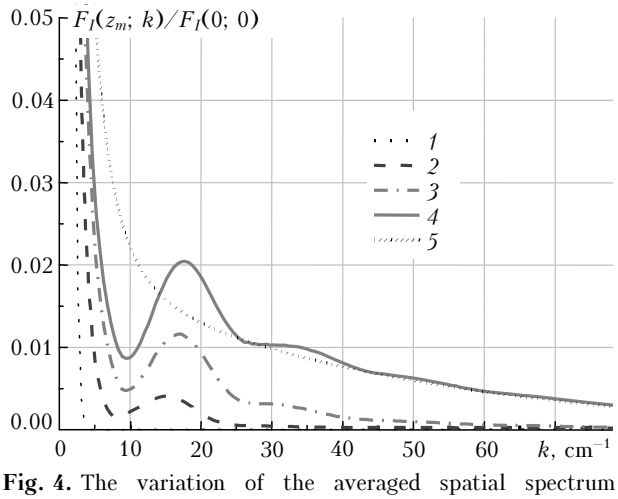


**Fig. 4.** The variation of the averaged spatial spectrum $F_I(z_m; k)/F_I(0; 0)$ at self-focusing in the rain for the following values of $z_m$: 1 (*1*), 50 (*2*), and 60 m (*3*), $\tilde{L}_{max}$ ($< \tilde{L}_{max} > = (62 \pm 3)$ m) (*4*); 69.4 m (*5*) in the absence of rain. Maximal dispersion of values is 10% (in the region of local maximum of the curve *4*).

Because of the scattering by rain droplets, the intensity distribution at self-focusing becomes

nonunimodal. A local maximum is formed in the spectrum, which increases with the distance. The local maximum frequency $k$ is about 15 cm$^{-1}$, that corresponds to the spatial scale $\Delta l \sim 2.1$ mm. The radiation power, falling on the area of such a perturbation, is about $1.9P_{cr}$. According to Ref. 13, such perturbations of light field have the largest increment in the Kerr medium. Therefore, further intensity increase in these areas can be expected. As the distance increases, the frequency of local maximum increases up to $k = 17.8$ cm$^{-1}$ ($\Delta l \sim 1.7$ mm), and the amplitude of these perturbations grows, determining the processes of energy redistribution in the beam and formation of filaments.

In the rain with a higher droplet concentration ($n = 1.7 \cdot 10^4$ m$^{-3}$) the formation of local maximum in the spatial spectrum $F_I(k)$ occurs more rapidly (Fig. 5*a*).

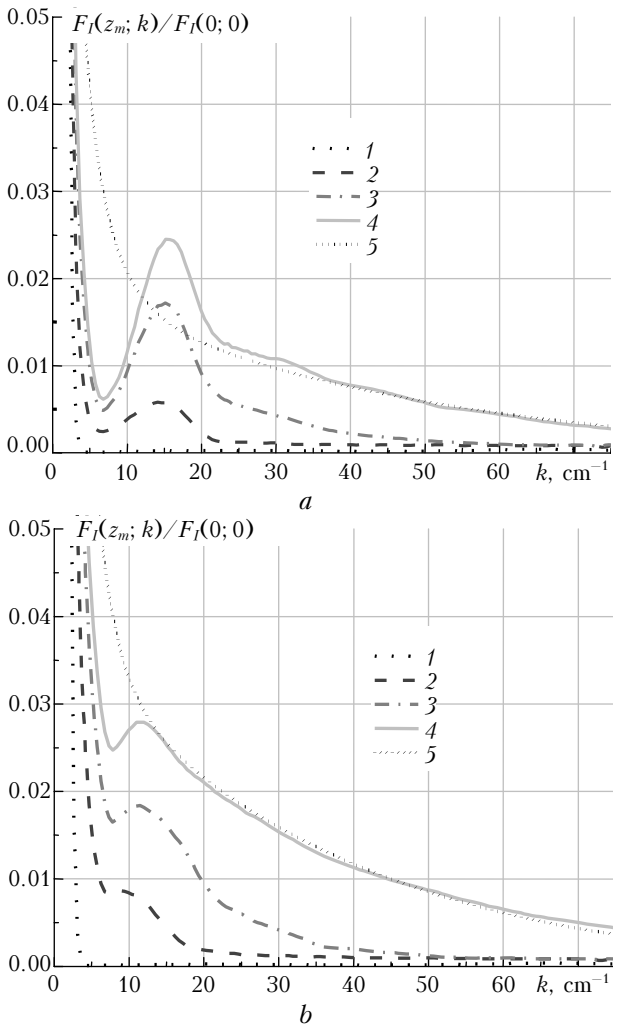


**Fig. 5.** The variation of the averaged spatial spectrum of beam intensity $F_I(z_m; k)/F_I(0; 0)$ at self-focusing in rain with the distance $z_m$ at $n = 1.7 \cdot 10^4$ m$^{-3}$. (*a*): $P = 100P_{cr}$, $z_m = 1$ (*1*), 40 (*2*), 50 m (*3*), $\tilde{L}_{max}$ ($<\tilde{L}_{max}> = (53 \pm 2)$ m) (*4*), 69.4 m in the absence of rain (*5*); (*b*): $P = 50P_{cr}$, $z_m = 1$ (*1*), 80 (*2*), 95 m (*3*); $\tilde{L}_{max}$ ($<\tilde{L}_{max}> = (97 \pm 3)$ m) (*4*); 102.2 m (*5*) in the absence of rain. The maximal dispersion of values is about 10% (in the region of curve *4* local maximum).

Its formation begins at smaller distances, and the amplitude reaches larger values than in aerosol of a lower concentration. Nevertheless, the spatial frequency with a local maximum practically does not vary. The spatial scale $\Delta l$ of dominating perturbations in the intensity distribution at $z_m = 40$ m is ~ 2.3 mm, and the power is about $2.3P_{cr}$. Thus, the increase of aerosol concentration results in somewhat earlier energy redistribution and, hence, accelerates the development of the small-scale self-focusing in a beam under conditions of the Kerr nonlinearity. Simultaneously, the increase of the local maximum amplitude shows the increase of the portion of distortions of the corresponding scale in the laser beam and, consequently, the growth of the number of "hot" points, that is, the number of the incipient filaments.

Note that the optical thickness $\tau$ of the path in the rain is low. At $n = 1.7 \cdot 10^4$ m$^{-3}$ $\tau \sim 0.14$. The pulse power extinction due to the scattering in the rain affects slightly the initial stage of filamentation, in contrast to the case of the dense dispersion layer considered in Ref. 11.

As the beam power decreases, the local maximum in the spatial spectrum is retained and shifted to lower frequencies (Fig. 5*b*), to which perturbations with the largest increment are corresponded. The power portion for the perturbations is ~ $1.8P_{cr}$. Note that in the low-frequency range ($k < 10$ cm$^{-1}$) the intensity spectrum broadening is less than in the case of self-focusing free of distortions. Hence, the beam perturbations due to scattering by rain droplets are favorable for the development of small-scale self-focusing, preventing the beam compression as a whole.

Figures 4 and 5 show spatial spectra for $\tilde{L}_{max}$, at which the peak intensity at a small-scale focusing more than 100 times exceeds the $I_0$ initial value. At the same $n$ and $P$ this distance varies within some limits from one realization to another. The mean length $<\tilde{L}_{max}>$ by 10 realizations for the case of $100P_{cr}$ is $(62 \pm 3)$ m at $n = 1.7 \cdot 10^3$ m$^{-3}$; and it decreases up to $<\tilde{L}_{max}> = (53 \pm 2)$ m with increasing $n$ to $1.7 \cdot 10^4$ m$^{-3}$. As the beam power decreases to $50P_{cr}$, $<\tilde{L}_{max}>$ also becomes much less than $z_{sf}$ and $L_{max}$ at the global self-focusing without aerosol. This is confirmed by the fact that in the rain the small-scale self-focusing occurs faster than the global one in the absence of aerosol. Hence, the earlier incipience and development of filaments can be expected under rain conditions.

## Conclusion

The initial stage of filamentation, when a high-power femtosecond laser pulse crosses the rain, has been numerically investigated. It is shown that the intensity perturbations occurring at interference of radiation scattered by drops, become the filamentation centers in the pulse, which peak power tens of times exceeds the critical power of self-focusing. The pattern of the intensity distribution in the pulse cross section corresponding to the short-exposition detection has

been obtained. The intensity distribution contains randomly located "hot" points positioning filaments, and ring formations due to the diffraction of light field by drops. Results of numerical simulation are in agreement with the data of the *in situ* experiment.[12]

Our studies revealed that there exists a transformation of the spatial intensity spectrum in a beam at the initial stage of filamentation. The spectrum becomes two-scaled, that indicated the development of perturbations due to the modulation instability in a high-power beam with distortions due to the coherent scattering by rain droplets. There appears a local maximum in the spectrum, whose position on the axis of spatial frequencies is determined by the perturbation with the largest increment and depends not on the aerosol concentration but only on the beam power. The local maximum amplitude increases with the growing particle concentration, that results in contracting the distance up to the filament incipience. Thus, the distance to the start of the filament formation in the pulse, whose power by a factor of several tens exceeds the self-focusing critical power, decreases in the rain with an extinction coefficient of several inverse kilometers.

## References

1. J. Kasparian, M. Rodriguez, G. Méjean, J. Yu, E. Salmon, H. Wille, R. Bourayon, S. Frey, Y.-B. André, A. Mysyrowicz, R. Sauerbrey, J.-P. Wolf, and L. Wöste, Science **301**, No. 5629, 61–64 (2003).
2. L. Bergé, S. Skupin, F. Lederer, G. Méjean, J. Yu, J. Kasparian, E. Salmon, J.-P. Wolf, M. Rodriguez, L. Wöste, R. Bourayon, and R. Sauerbrey, Phys. Rev. Lett. **92**, No. 22, 225002:1–4 (2004).
3. S.A. Hosseini, Q. Luo, B. Ferland, W. Lin, S.L. Chin, O.G. Kosareva, N.A. Panov, N. Aközbek, and V.P. Kandidov, Phys. Rev. A **70**, No. 3, 033802:1–12 (2004).
4. S.A. Shlenov and V.P. Kandidov, Atmos. Oceanic Opt. **17**, No. 8, 565–570; 571–575 (2004).
5. V.P. Kandidov and V.O. Militsin, Atmos. Oceanic Opt. **17**, No. 1, 46–53 (2004).
6. A.A. Zemlyanov and Yu.E. Geints, Atmos. Oceanic Opt. **18**, Nos. 1–2, 53–60 (2005).
7. F. Courvoisier, V. Bouton, J. Kasparian, E. Salmon, G. Méjean, J. Yu, and J.-P. Wolf, Appl. Phys. Lett. **83**, No. 2, 213–215 (2003).
8. M. Kolesik and J.V. Moloney, Opt. Lett. **29**, No. 6, 590–592 (2004).
9. N.N. Bochkarev, Al.A. Zemlyanov, A.A. Zemlyanov, A.M. Kabanov, D.V. Kartashev, A.V. Kirsanov, G.G. Matvienko, and A.N. Stepanov, Atmos. Oceanic Opt. **17**, No. 12, 861–864 (2004).
10. G. Méjean, J. Kasparian, J. Yu, E. Salmon, S. Frey, J.-P. Wolf, S. Skupin, A. Vincotte, R. Nuter, and S. Champeaux, Phys. Rev. E **72**, No. 2, 026611:1–7 (2005).
11. A.A. Zemlyanov and Yu.E. Geints, Opt. Commun. **259**, Is. 2, 799–804 (2006).
12. G. Méchain, G. Méjean, R. Ackermann, R. Rohwetter, Y.-B. André, J. Kasparian, B. Prade, K. Stelmaszczyk, J. Yu, E. Salmon, W. Winn, S.A. Schlie, A. Mysyrowicz, R. Sauerbrey, L. Wöste, and J.-P. Wolf, Appl. Phys. B. **80**, No. 7, 785–789 (2005).
13. V.I. Bespalov and V.I. Talanov, Pis'ma Zh. Eksp. Teor. Fiz. **3**, No. 12, 471–475 (1966).
14. V.O. Militsin, L.L. Kuzminskii, and V.P. Kandidov, Atmos. Oceanic Opt. **18**, No. 10, 789–795 (2005).
15. L.L. Chin, L. Petit, W. Liu, A. Iwasaki, M.-C. Nadeau, V.P. Kandidov, O.G. Kosareva, and K.Yu. Andrianov, Opt. Commun. **210**, Is. 4, 329–341 (2002).
16. V.E. Zuev and M.V. Kabanov, *Optics of Atmospheric Aerosol* (Gidrometeoizdat, Leningrad, 1987), 246 pp.
17. V.P. Kandidov, O.G. Kosareva, E.I. Mozhaev, and M.P. Tamarov, Atmos. Oceanic Opt. **13**, No. 5, 394–401 (2000).
18. J.H. Marburger, Prog. Quantum Electron. **4**, No. 1, 35–110.35 (1975).